



LAWRENCE
LIVERMORE
NATIONAL
LABORATORY

Systems considerations for Resonance-Ionization Mass Spectroscopy in the application of Nuclear Forensic Analysis by Ray Mariella Jr

R. P. Mariella

July 26, 2012

Disclaimer

This document was prepared as an account of work sponsored by an agency of the United States government. Neither the United States government nor Lawrence Livermore National Security, LLC, nor any of their employees makes any warranty, expressed or implied, or assumes any legal liability or responsibility for the accuracy, completeness, or usefulness of any information, apparatus, product, or process disclosed, or represents that its use would not infringe privately owned rights. Reference herein to any specific commercial product, process, or service by trade name, trademark, manufacturer, or otherwise does not necessarily constitute or imply its endorsement, recommendation, or favoring by the United States government or Lawrence Livermore National Security, LLC. The views and opinions of authors expressed herein do not necessarily state or reflect those of the United States government or Lawrence Livermore National Security, LLC, and shall not be used for advertising or product endorsement purposes.

This work performed under the auspices of the U.S. Department of Energy by Lawrence Livermore National Laboratory under Contract DE-AC52-07NA27344.

Systems considerations for **Resonance-Ionization Mass Spectroscopy** in the application of Nuclear Forensic Analysis

by Ray Mariella Jr.

July 2012

This work performed under the auspices of the U.S. Department of Energy by Lawrence Livermore National Laboratory under Contract DE-AC52-07NA27344.

Normally, a full Systems-Engineering Review of an instrument used in any process is rather involved, starting with *Stakeholder Expectations, Technical Requirements, Scenarios of Use, Concept of Operations, etc.*, as described, for example, in several NASA documents, such as NASA Procedural Requirements NPR_7123.1 and NASA/SP-2007-6105, two of which are available for download on the web [<http://nodis3.gsfc.nasa.gov/displayDir.cfm?t=NPR&c=7123&s=1A> and <http://education.ksc.nasa.gov/esmdspacegrant/Documents/NASA%20SP-2007-6105%20Rev%201%20Final%2031Dec2007.pdf>].

Two figures are excerpted, below, including Figure 2.1-1, which is a general overview:

2.1 The Common Technical Processes and the SE Engine

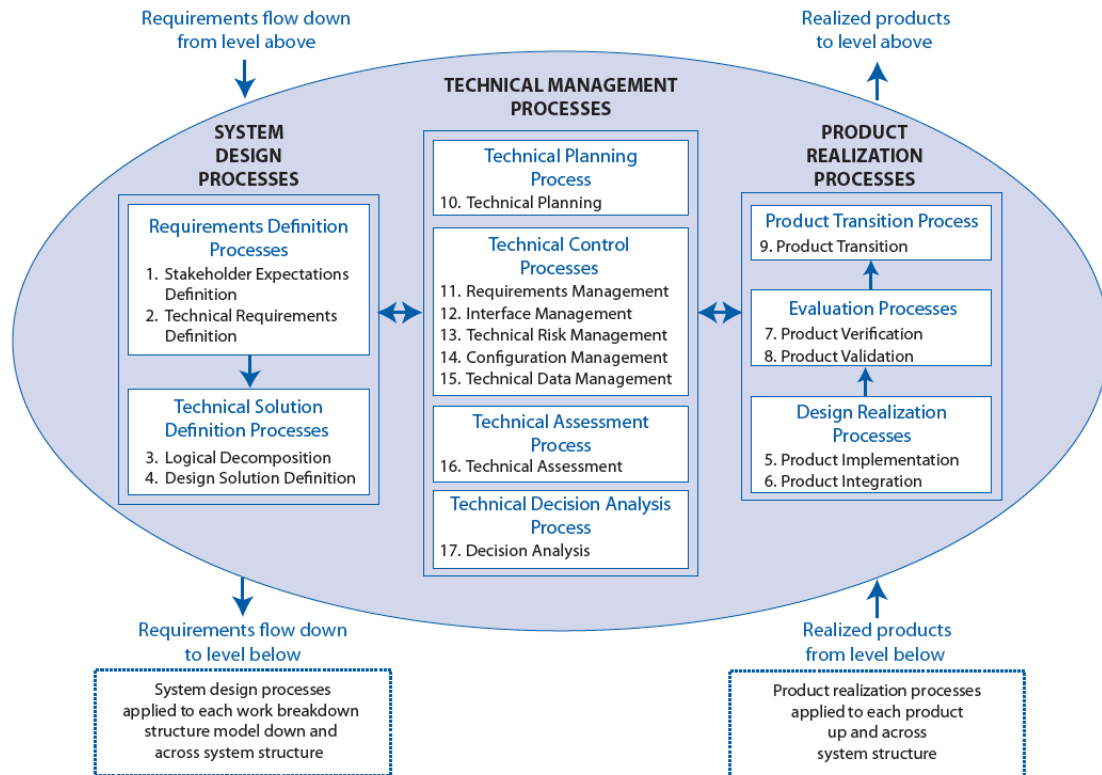


Figure 2.1-1 The systems engineering engine

Figure 1. Overview for the Process of System Engineering by NASA

A key element of the Technical Management Process, outlined below in Figure 6.4-1, is Technical Risk Management, which is part of the Technical Planning Process.

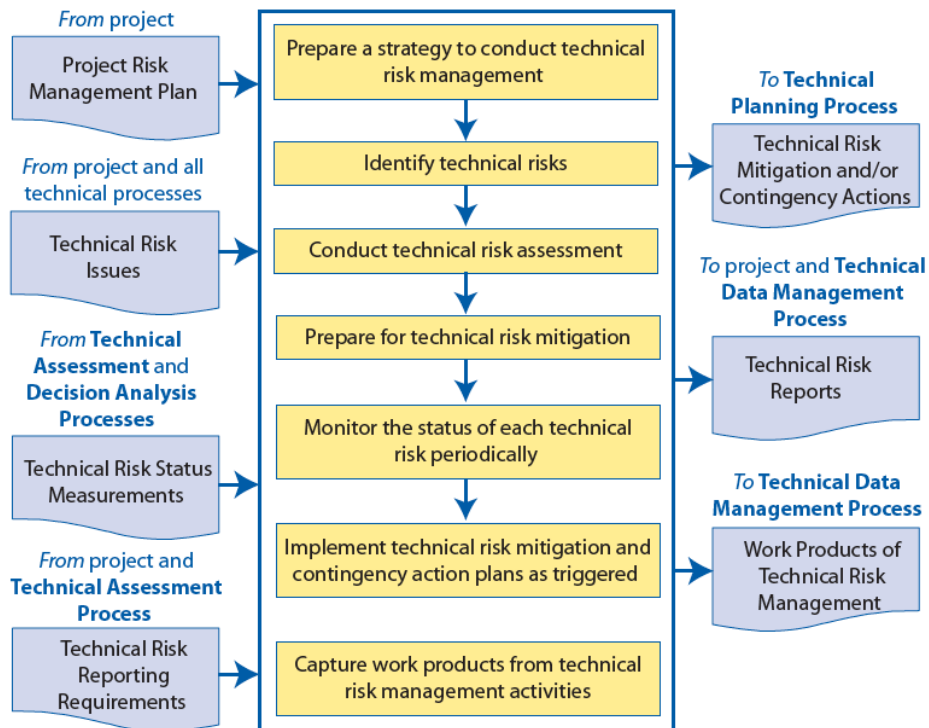


Figure 6.4-1 Technical Risk Management Process

140 • NASA Systems Engineering Handbook

Figure 2. Overview for the Process of Technical Risk Management by NASA

Because the Customer Expectations and other Stakeholder Expectations, along with Performance Specifications, are not yet fully-defined, a full System Engineering procedure cannot be performed at this time. The Appendix contains some thoughts about Technical Risk and possible Mitigation strategies.

Overview

Example Instrument Schematic for Resonance-Ionization Mass Spectroscopy ["RIMS"]

Analyzing presolar grains with CHARISMA

3217

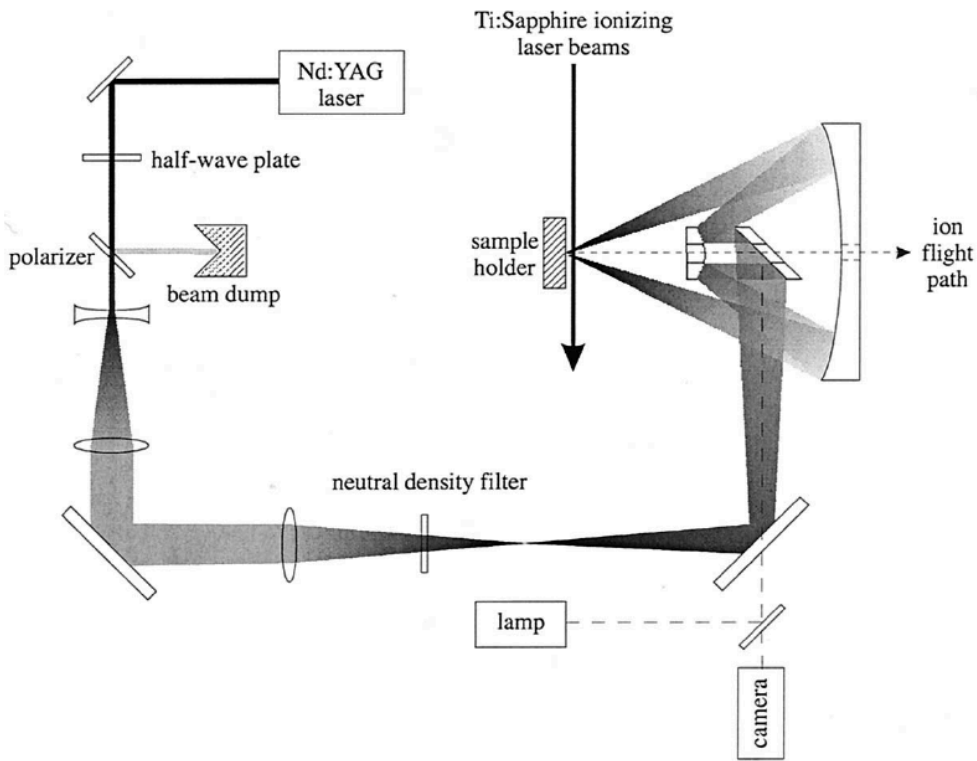


Fig. 2. Schematic drawing of the desorption laser beam path. See discussion in text.

Figure 3. Schematic of Argonne National Lab RIMS instrument, shown using Nd:YAG laser ablation to generate atoms of interest⁷

Simplified Timing Sequence to Collect RIMS Data from Solid Target:

STEP 1

Generate vapors that contain *ground-state* atoms of the element[s] of interest:

1. Thermal [evaporative] source [heated filament used for this]
2. Laser ablation [typically a few- μm spot size, rastered spot. This is a highly non-linear process with a threshold. Typical laser requirements are ≈ 50 kJ/g ablated for oxides, depending upon the nature of the sample and sample surface. The ground-state atoms would be a small fraction of the total amount of ablated material.
3. Pulsed, ion-beam sputter [typically μm or smaller size, 10's of nA current, 25 keV, rastered spot] generates $\approx 10^5$ atoms/pulse. Amount of material sputtered is roughly linear in ion-beam current for fixed ion energy. The ground-state atoms would be a small fraction of the total amount of ablated material.

If the vapor-generation process collaterally generates ions, then a transient E field is used to remove these ions, prior to the next step of selective excitation of atoms with laser.

Engineering Considerations for STEP 1

Laser ablation, compared with ion-beam sputtering, is a process that is highly non-linear and very surface-dependent, but is capable of ablating large amounts of material and, depending upon circumstances, can generate a higher fraction of atoms from molecular sources. In a limited RIMS study, a 193-nm ArF excimer laser was used to produce neutral Sn atoms efficiently from a compound⁸. [It is unclear if this study by Atom Sciences, a spin-off of the RIMS work at Oak Ridge National Lab, will transfer to LLNL interests in actinides. However, each 193-nm photon carries 6.4 eV of energy, which is enough to break most bonds and might, therefore, increase the fraction of U over UO_x in laser ablation RIMS.]

STEP 2

Quantitatively, excite atoms of the element[s] of interest [e.g., U] from their ground state to an electronically-excited state^{2,9}, U^*

Engineering Considerations for STEP 2

In general, it maximizes performance to direct the excitation and photoionization laser beams close and parallel to the surface being ablated/sputtered. If either of those beams struck the surface, directly, it would likely cause further ablation of the target, which could confound the step of timed removal of undesired ions, could cause the loss of some remaining atoms of interest from the main detection process, and could introduce off-normal or difficult-to-characterize signals.

Choosing the areas and shapes of the exciting and ionizing laser beams above the surface is part of the process of optimization, based on the expansion of the ablated/sputtered material and the dimensions and throughput of the ion optics and mass spectrometer¹⁰ [see p70 of B. Isselhardt thesis]. Immediately at the surface, the nascent cloud of ablated/sputtered matter has the density of the solid target [$n \approx 2.3 \times 10^{22}$ molecules/cm³]

for UO_2 , $n \approx 2.5 \times 10^{22}$ molecules/cm³ for SiO_2] and is a location in which collisions between atoms of interest and all other constituents can be frequent, [mean free path $\approx 1/n\sigma$, where σ is the collision cross section, $\approx 6 \times 10^{-15}$ cm², gives m.f.p. ≈ 0.2 nm for neutral collisions at \approx solid density]

Assuming the ablation laser delivered ≈ 30 nJ, needing $\approx 5 \times 10^4$ J/g to ablate would mean ≈ 600 fg ablated/laser pulse. If the material were pure UO_2 , then $\approx 1.4 \times 10^{10}$ molecules, such as UO_2 , would be ablated. During the earliest phase of expansion, a uniform density of molecules can be assumed to fill the expanding hemisphere, and when the expanding plume of ablated molecules extends only 0.5 mm from the surface, the density has dropped to 6×10^{13} /cm³ and the m.f.p. ≈ 3 cm, which means that if the excitation and ionization lasers are ≈ 0.5 mm above the sample, then collisions of neutrals [and undesired collisional energy transfer or even charge-changing collisions] will be rare events.

Again, the countering motivation is that one wants to locate the laser beams as close to the target surface as possible, because this minimizes the size of the apparent ion source from the photoionization process and, hence increases the performance of the ion optics and mass spectrometer.

These numbers are obviously rough estimates, but can serve as guidelines.

Depending upon spectroscopic details^{2,9}, the generation of U^* could be a one- or two-photon process. A one-step excitation of U atoms, for example, could use 436.3-nm light, but the subsequent photoionization step would require 367.9-nm light, which would cause more non-specific ionization of other constituents. For U atoms, two-step excitation could use 415.5-nm and 829.1-nm light. Because U isotopes with odd number of neutrons have a nuclear magnetic moment and, hence, higher degeneracies of energy levels, correction terms must be included to compensate for differing excited-state population densities than would be obtained if all isotopes had the same degeneracies of energy levels. See Isselhardt thesis¹⁰, p 87, and Schumann, et al.¹¹

The spray^{12,13} of atoms, molecules, and clusters from STEP 1 [roughly cosine distribution from ion-beam sputtering¹² and narrower, bimodal ($a \cos^m\theta + (1 - a) \cos^n\theta$) distributions¹³ were seen in laser ablation of SrZrO_3] carries with it Doppler shifts for the interaction of atoms of interest with the nominally-perpendicular laser beams. Doppler broadening is an inhomogeneous mechanism, which means that U atoms with different velocity components parallel to the laser beam will exhibit peak resonances at different wavelengths¹⁴. This effect is easily seen with spectroscopy of isotope shifts in atomic beams¹⁵.

Since the isotope shift in U atoms exceeds the Doppler width, if the bandwidth of the excitation laser is broad enough to excite all isotopes of interest, it will cover the broadening due to the Doppler effect, as well¹⁶. By using a laser with an intentionally-broadened bandwidth, the effects of power broadening can largely be ignored^{17,18}.

Since most laser beams from commercial lasers have Gaussian spatial profiles, there is likely to be an optimization process regarding the nominal beam sizes of the excitation laser beam[s]. Increasing the laser intensity, for a fixed, nominal beam width, will increase the number of U^* atoms at the outside regions of the first excitation beam [415.5 nm]. Assuming that the subsequent excitation and photoionization lasers were collinear and overlapping [possibly with larger beam diameters], then the U^* atoms in the lower-

intensity annulus of the 415.5-nm laser beam could be excited a second excited state and ionized. If the ion extraction optics and mass spectrometer detect these ions, then the signal is increased. However, the tradeoff is that increasing the intensity of the 415.5-nm laser will also increase the non-specific ionization of atoms or molecules.

If performing multiplexed assay, such as U and Pu, one could alternate the laser wavelengths in STEP 2, exciting only U or Pu atoms at any one time and repeat until the S/N is acceptable. If a pre-screen indicates a great excess of either U or Pu, one could increase the duty cycle for the minor element over that for the major.

STEP 3

Quantitatively, photoionize U* atoms, only. [Ionization potential of U \approx 6.2 eV]

Engineering Considerations for STEP 3

Minimize non-specific photoionization, excitation¹⁹ or charge-changing collisions, etc., all of which give can spurious and possibly confounding signals.

To maximize throughput and yield, it is important to match excitation/ionization volume to the extraction aperture of the mass spectrometer.

Some atoms, including U, do not need to be excited directly into the free-electron continuum for photoionization [$\sigma \approx 10^{-18} \text{ cm}^2$ or smaller^{20,21}], but possess autoionizing states² that exhibit much larger cross sections [$\sigma \approx 10^{-15} \text{ cm}^2$] for absorption of ionizing photons. From the Paisner&Solarz RIMS studies² in 1976: “We have found that the uranium photoionization spectrum is heavily dominated by autoionization, with the cross section for ionization varying by over two orders of magnitude.”

The presence of a resonant, autoionizing state significantly reduces the power requirements for the photoionization laser and the reduced power reduces the very undesirable, non-specific¹⁹ photoionization. The kinetics of the coupled steps has been discussed by B. Isselhardt in his thesis¹⁰, but, in short, if the rate of photoionization exceeds the duration of the excitation and photoionization pulses, and the Rabi frequency of the excitation process between the ground state and the upper excited state is rapid enough to replenish the upper state population that is depleted by the photoionization, then most, if not all, of the ground-state atoms that are illuminated by the laser beams can be ionized for extraction into the mass spectrometer.

STEP 4

Use electric field to extract photoionized atoms into the mass spectrometer. Measure and record isotopic abundances.

Engineering Considerations for STEP 4

The physical volume of the photoionized U inherently contains a component along the direction of extraction, which causes a spread in the initial energy of ions as a function of location between the plates with extraction voltage. A reasonable work-around has been

employed by the LLNL/Argonne team, which is to apply the extraction voltage in two stages, where the second voltage is greater than the first. The absolute spread of initial energies is thereby made a smaller percentage of the total voltage. There is inevitably a tradeoff between efficiency/throughput of the mass spectrometer and its resolution. The existing reflectron time-of-flight instrument used at Argonne has not baseline-resolved all isotopes of U and a similar resolution and mass range is needed for Pu. It may be necessary to do a redesign or replacement with a mass spectrometer that uses a different type of mass filter [Mattauch-Herzog, etc.].

Multiplex Option

If there are no isobaric interferences, it may be possible to add excitation laser wavelengths to excite and ionize more than one element at a time. This, of course, increases the complexity of the instrument. More excitation photons would also mean increased non-specific photoionization, possible excitation or charge-changing collisions, but these effects can be minimized and, possibly, subtracted from the resonant signals, with wavelength-agile excitation lasers. Elements that could possibly be measured with RIMS are shown, below.

Fission Products	Actinides	Activation Products
72-Zn	234,235,236,237,238,240-U	55,59-Fe
77-As	239-Np	57,58,60-Co
79-Se	238,239,240,241,242-Pu	72-Ga
89,90-Sr	240,241-Am	160-Tb
91-Y	242-Cm	181,185,187,188-W
95,97-Zr		210-Pb
99-Mo		
111,112-Ag		
115,115m-Cd		
129m,132-Te		
136,137-Cs		
140-Ba		
141,143,144-Ce		
147-Nd		
149/151-Pm		
153-Sm		
156-Eu		
161-Tb		

Brief History of Resonance Ionization Spectroscopy and Resonance Ionization Mass Spectroscopy

Although resonance-ionization spectroscopy [“RIS”] has been known for more than 40 years¹, and RIMS was demonstrated 38 years ago²⁻⁶, the instrumentation that performs RIMS continues to improve, driven both by advances in lasers and by advances in Data acquisition and computers and control electronics. Tunable, Ti:Sapphire lasers, which are pumped by doubled Nd:YLF or similar lasers, are the preferred source to excite resonant atomic transitions, today, but there is every reason to believe that, in time, lasers will become available that will decrease the size and weight of a RIMS system, and make it more portable. For example, GaN-diode-laser-pumped Ti:sapphire could offer higher repetition rates and smaller size.

The earliest work with RIS and RIMS used thermal-evaporative sources to generate gas-phase atoms: in 1971, Ambatzumian and Letokhov¹ used a pulsed ruby laser with dye laser to excite Rb atoms and the doubled-ruby-laser output to ionize the Rb* atoms [this document follows the standard notation that X* denotes electronically-excited X]. In 1974, Tuccio and Peterson³ at LLNL used a cw dye laser with a mercury arc lamp to ionize the U*. In 1976, Paisner, Solarz, and colleagues at LLNL performed RIMS on U vapor², where the mass spectrometer was used to discriminate against non-specific, multi-photon ionization of UO and UO₂. This early RIMS work used a simple thermal oven to produce ground-state U atoms. In 1980, however, Hurst and colleagues at Oak Ridge National Lab used pulses from a Q-switched Nd:glass laser to vaporize potassium target material, followed by a pulsed N₂-laser-pumped dye laser, operating at 404.4 nm, both to perform resonance excitation [4s to 5P] and to photoionize the resultant K* atoms.

By 1983, Donohue, at ORNL, using a heated filament to vaporize the metal, applied RIMS to the detection of Pu²². In 1984, Donohue also measured isotope ratios of Pu and U in mixtures²³, and was considering the influence of excitation-laser bandwidth on the process²⁴, which has been elegantly studied, more recently by the LLNL&Argonne team¹⁶. Trautmann & co-workers applied RIMS to nine Actinides^{25,26}.

In 1988, Goeringer et al., at ORNL, investigated matrix effects for production of ground-state U atoms from a variety of targets²⁷, and concluded “This relatively large matrix effect severely limits the applicability of SA/RIMS to quantitative analysis of uranium samples.”

Although performed more than a decade ago, this shows that RIMS continues to have opportunities for study and improvement, and, for example, is being addressed by Kim Knight, at LLNL²⁸, who studied the production of ground state U atoms from cuprosklodowskite²⁸, a naturally-occurring ore that contained 23% U. Dr. Knight found that laser-ablation produced a higher fraction of ground-state U atoms than Ga⁺ ion-beam sputtering, which Goeringer, et al., used²⁷. As mentioned, above, surface ablation with a 193-nm [ArF excimer] laser⁸ may increase the U/UO_x ratio, further.

Moreover, the missions of Nuclear Forensics do not necessarily demand limits of detection [“LOD”] low enough to detect natural U in soil or building materials, but rather

LOD's low enough to detect unburned nuclear fuel, fission products, activation products, and similar elements in fallout, with uncertainties of isotopic ratios on the order of 1% or smaller. Naturally-occurring uranium is found in soils²⁹ and building materials, such as granite and sandstone²⁹, along with Portland cement³⁰, typically at 10's of ppm concentration^{31,32}. Thus, even if 20% of a RIMS signal originated from underlying debris/rubble that contained 10 ppm natural uranium [99.3% ²³⁸U], its contribution to the ratio 235/238 for enriched material that contained 5% or more U would be far less than 1%. Similar considerations apply to the 234/238 and 236/238 ratios. If the high spatial resolving power of RIMS [either with ion-beam sputtering or laser-ablation to generate the ground-state atoms] can examine fallout particles and not distract itself analyzing the remainder of debris that carried the fallout particle, then the RIMS performance in measuring U and Pu isotope ratios can be good. Given the heterogeneous nature of the samples, some rapid, wavelength-switchable resonance ionization between U and Pu would be needed, since both cannot be analyzed simultaneously, under the current configuration.

A recent example of the two-step excitation of U, with wavelengths of 415.5 nm and 829.1 nm, followed by 722.2-nm excitation to an autoionization state, is shown schematically, below¹⁶.

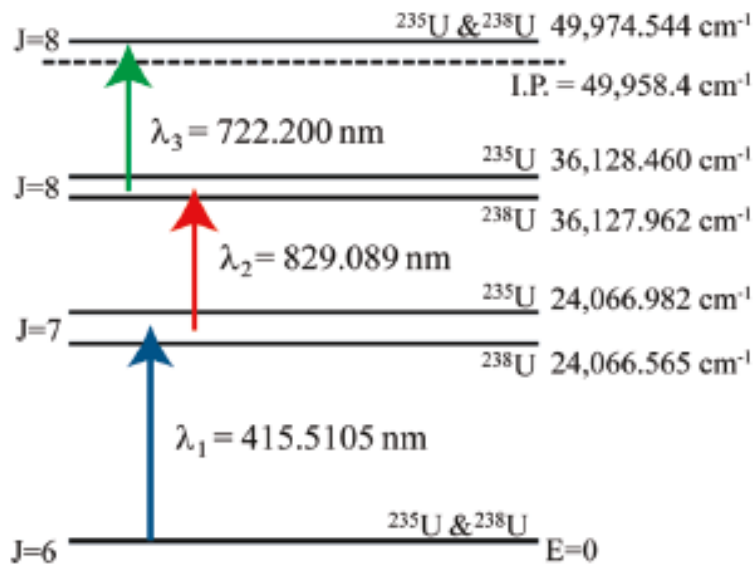


Figure 2. The three-color, three-photon resonance ionization scheme used in this work (adapted from Schumann et al.¹⁸) displays the difference in atomic transitions due to the isotope shifts for ²³⁵U and ²³⁸U at each resonance, along with the corresponding average wavelength. For the high-lying excited states, only the angular momentum and parity are known.

Interferences

RIMS is based on the assumption that other potentially interfering species will mostly remain unexcited in the irradiation volume of the laser beams.

UO and UO₂ have ionization potentials, 5.6 and 5.8 eV, respectively³³, that would require at least 2 photons at 415 nm to photoionize, and this non-resonant photoionization rate would be proportional to the square of the laser intensity. Ground-state Pu, with ionization potential of ≈ 6 eV, would also require two 415.5-nm photons for photoionization process which would, again be proportional to the square of the laser intensity at 415.5 nm. At least three photons of 722-nm wavelength would be required to photoionize ground-state Pu, as well as UO and UO₂. This process would be proportional to the cube of the laser intensity at 722 nm.

When Pu is being excited and photoionized, there may be a small signal from non-resonant photoionization of a low-lying metastable states³⁴ of U [$f^6ds^2(^5K_5^0)$ and $(^5L_7^0)$] that are very likely to be populated by either the ion-sputtering process or laser ablation. Kim Knight observed that only a small percentage of sputtered or ablated atoms are ground-state U; most are UO and UO₂, but percentage yields of ground-state U atoms was higher with laser desorption than with Ga⁺ ion sputtering²⁸.

Broadening of the 415 excitation and 829 nm lasers, which is used by the LLNL/Argonne team, today¹⁶, is more technically feasible than simultaneously injecting individual lines tuned to each isotope's wavelength into an amplifier, however the consequence is that there are more photons in the excitation volume that can perform non-specific photoionization; this is a very small effect, under the current circumstances.

Appendix – Technical Risks

Considerations of how to match the high spatial resolution and low throughput of RIMS to arbitrary debris samples that contain mm-scale or smaller fallout particles:

μ -X-ray-fluorescence^{35,36} prescreening of multi-gram samples after a detonation could identify the μ m-scale spots where the device components condensed, which would enable the spatially-accurate analytical capabilities of RIMS to extract important information, such as U and Pu isotopic composition. Although rapid μ -XRF, today, employs synchrotron radiation, there is every reason to believe that the technology of table-top X-ray sources³⁷ will continue to advance so that a fieldable system may be produced, within the next decade.

Recent examples of X-ray microprobe analysis for actinides are shown, below.

e.g., 2-D elemental maps from Denecke³⁵:

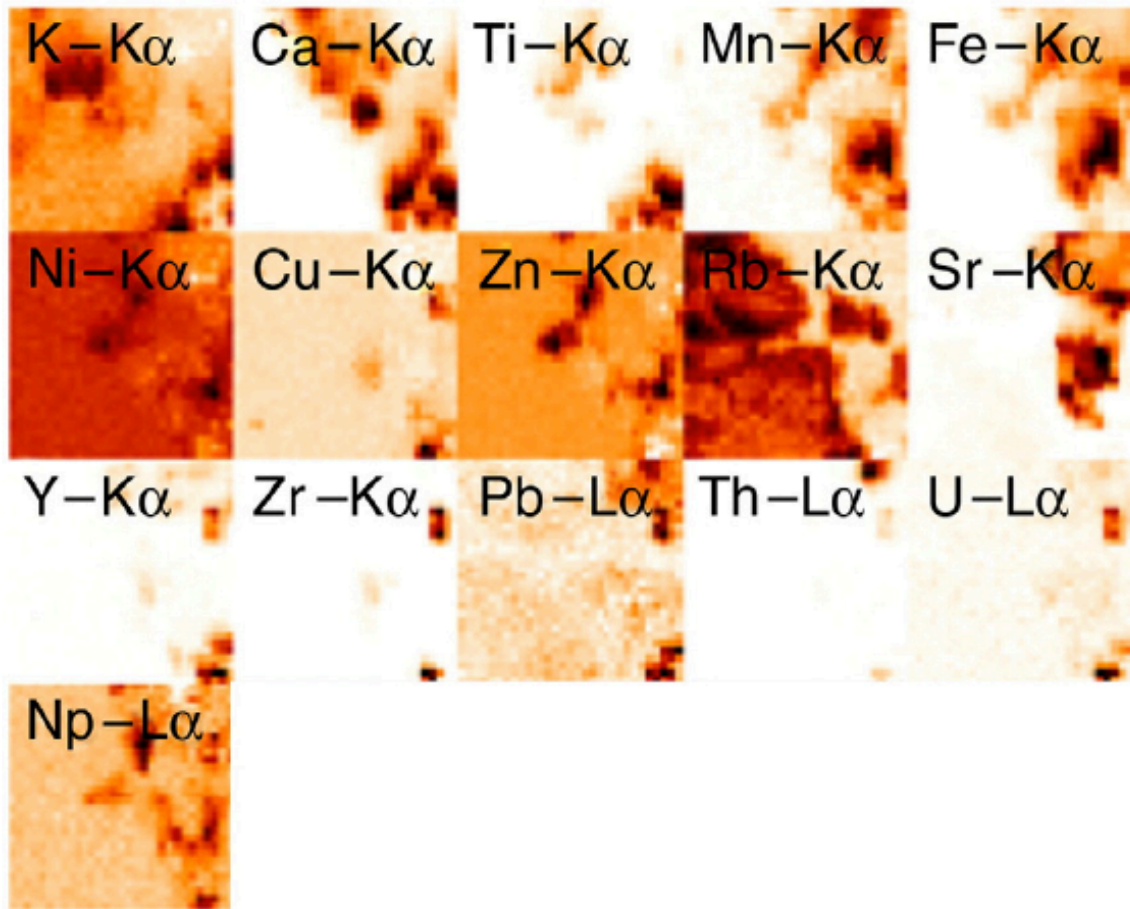


Fig. 2. Elemental distributions for the elements indicated for a 300 μm X 300 μm area of the granite section recorded \approx 58 μm below the surface. Scanning step size = 10 μm . Counting time = 5 s.

2-D elemental maps from Denecke³⁶:

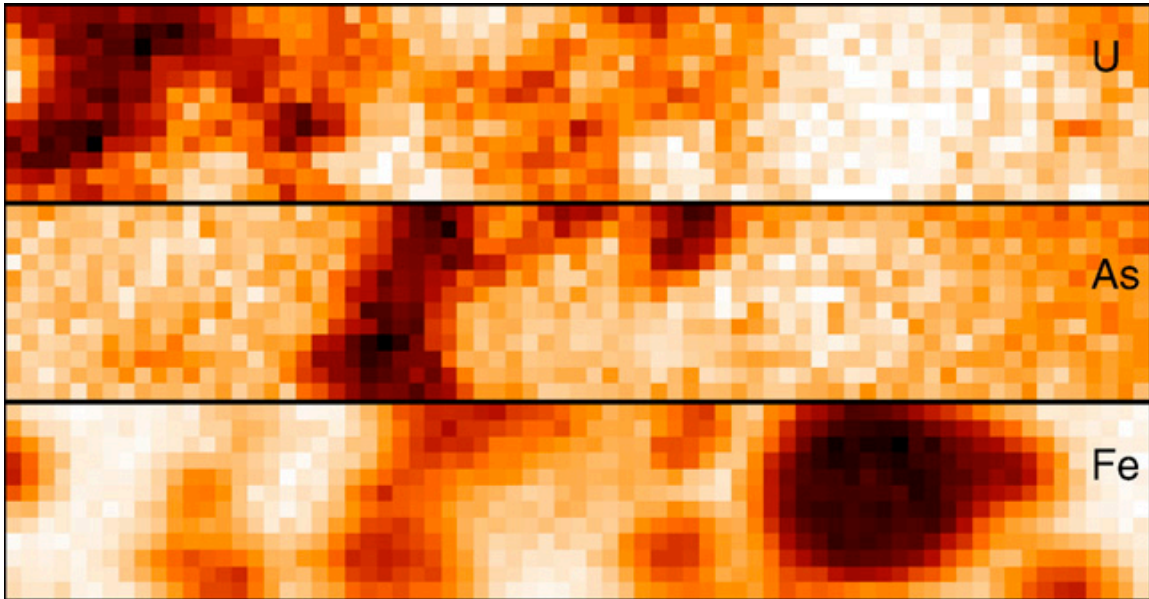


Fig. 3. Elemental distributions for Fe, As, and U recorded in the 710 μm x 120 μm area. Each pixel 10 μm x 10 μm . Counting time=10 s. Dark pixels represent areas of relatively high concentration and lighter pixels areas of low concentration, and white of no detectable concentration.

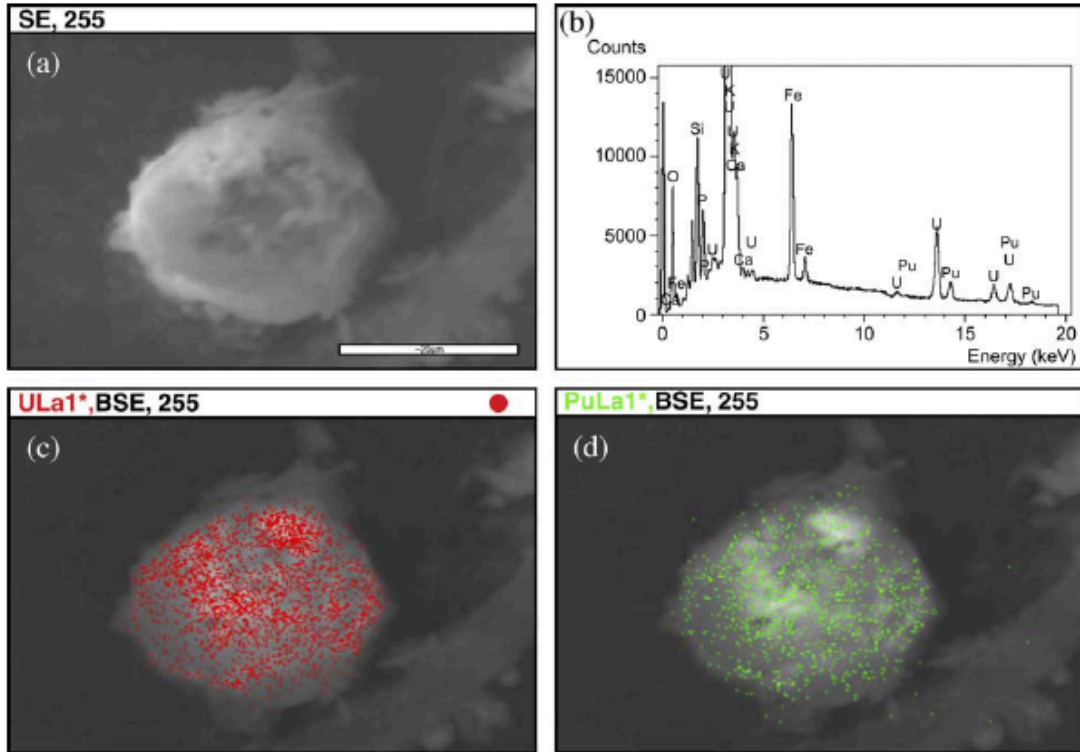
ref³⁸ Dahlgaard 2005

Fig. 2. Scanning electron microscopy of particle #132a in SEI-mode (a), elemental spot analysis by XRMA (b) and X-ray mapping of uranium (c) and plutonium (d) superimposed on a BEI mode image (Bar 20 μm).

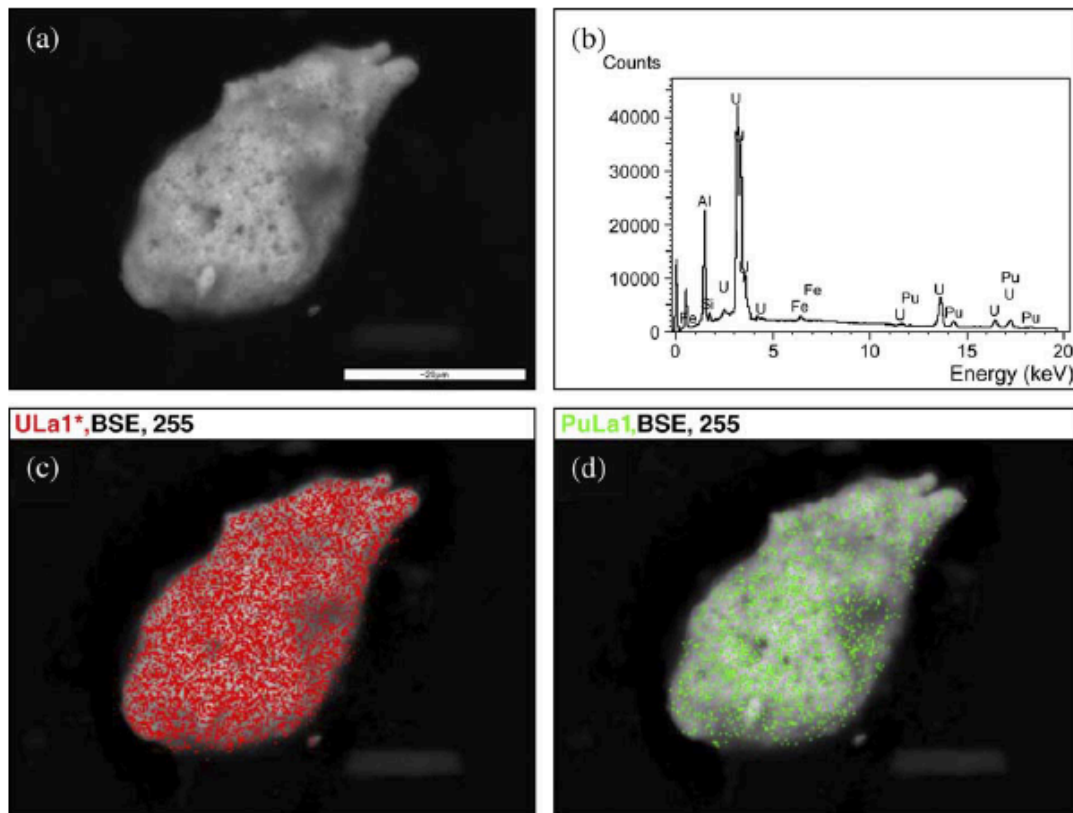


Fig. 3. Scanning electron microscopy of particle #133 in BEI mode (a), elemental spot analysis by XRMA (b), and X-ray mapping of uranium (c) and plutonium (d) superimposed on the BEI mode image (Bar 20 µm).

RIMS analysis of Pu, U, from Erdmann and Trautmann³⁹, shows the spatial resolving power of RIMS, in their study of radioactive particles, previously mapped by others^{38,40,41}, from the Thule, Greenland, nuclear incident:

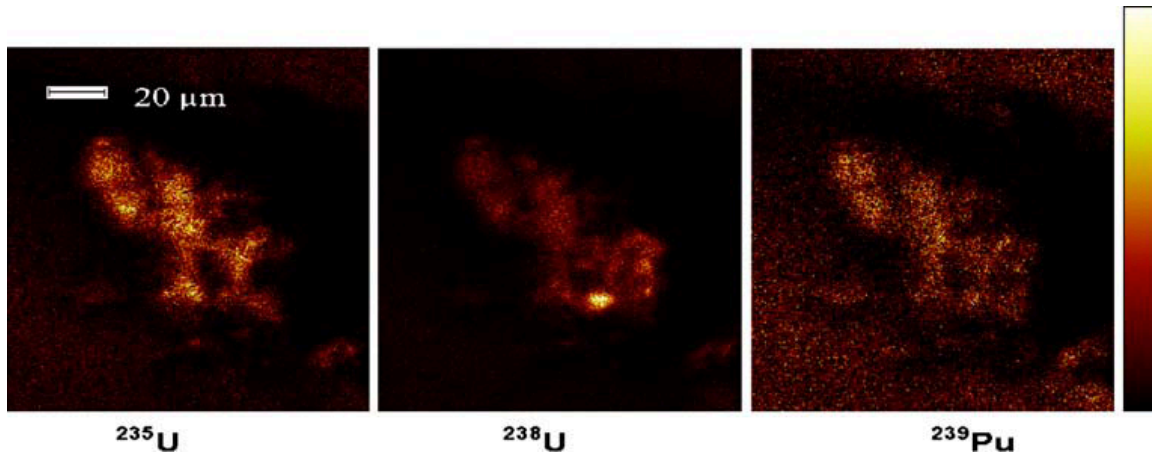


Fig. 3 Lateral distribution of ^{235}U , ^{238}U , and ^{239}Pu in a “Hot Particle” from Thule, determined by TOF-SIMS. The relative ion intensity in each pixel is visualized by a color scale from black/red (low intensity) to yellow (high intensity)

From Erdmann and Trautmann³⁹,

As a result of this accident, fissile material (enriched uranium and plutonium) contained in the bombs and depleted uranium from the casing was released and traces of this material can still be found in the environment, for example in sediment samples.

From such samples, a number of sediment particles with high concentrations of uranium and plutonium attached were identified and characterized by a number of analytical techniques^{38,40,41}. The particles had been transferred to separate sample holders, which contained marks that enabled a re-location of the particle with the various analytical methods.

One can clearly see different distributions for the different isotopes: the fissile ^{235}U and ^{239}Pu , which originate from the core of the bomb, show a similar and rather homogenous spatial distribution over the whole sediment particle, while ^{238}U , which is used in the outside shielding, is concentrated only in a small spot on the particle. **This example demonstrates the relevance of high spatial resolution (sub- μm) for these types of analyses, averaging over the whole particle would have resulted in a wrong $^{235}\text{U}/^{238}\text{U}$ ratio and loss of information.**

This last sentence [font made red for emphasis] highlights the value of applying the high spatial resolution of RIMS to such a problem.

References

1. Ambartzumian, R.V. & Letokhov, V.S. Selective Two-Step (STS) Photoionization of Atoms and Photodissociation of Molecules by Laser Radiation. *Appl. Opt.* **11**, 354-358 (1972).
2. Carlson, L.R., *et al.* RADIATIVE LIFETIMES, ABSORPTION CROSS-SECTIONS, AND OBSERVATION OF NEW HIGH-LYING ODD LEVELS OF U-238 USING MULTISTEP LASER PHOTOIONIZATION. *Journal of the Optical Society of America* **66**, 846-853 (1976).
3. Tuccio, S., Dubrin, J., Peterson, O. & Snavely, B. Two-step selective photoionization of ²³⁵U in uranium vapor. *Quantum Electronics, IEEE Journal of* **10**, 790-790 (1974).
4. Donohue, D.L., Young, J.P. & Smith, D.H. Determination of Rare-Earth Isotope Ratios by Resonance Ionization Mass-Spectrometry. *International Journal of Mass Spectrometry and Ion Processes* **43**, 293-307 (1982).
5. Beekman, D.W., *et al.* Resonance Ionization Source For Mass-Spectroscopy. *International Journal of Mass Spectrometry and Ion Processes* **34**, 89-97 (1980).
6. Kramer, S.D., *et al.* Applications of Resonance Ionization Spectroscopy to Ultralow-Level Counting and Mass-Spectroscopy. *Radiocarbon* **22**, 428-434 (1980).
7. Savina, M.R., *et al.* Analyzing individual presolar grains with CHARISMA. *Geochim. Cosmochim. Acta* **67**, 3215-3225 (2003).
8. Arlinghaus, H.F., Kwoka, M.N., Guo, X.-Q. & Jacobson, K.B. Multiplexed DNA Sequencing and Diagnostics by Hybridization with Enriched Stable Isotope Labels. *Anal. Chem.* **69**, 1510-1517 (1997).
9. Blaise, J. & Radziemski, L.J. ENERGY-LEVELS OF NEUTRAL ATOMIC URANIUM (UI). *Journal of the Optical Society of America* **66**, 644-659 (1976).
10. Isselhardt, B.H. Quantifying Uranium Isotope Ratios Using Resonance Ionization Mass Spectrometry: The Influence of Laser Parameters on Relative Ionization Probability. *Thesis* (2011).
11. Schumann, P.G., Wendt, K.D.A. & Bushaw, B.A. High-resolution triple-resonance autoionization of uranium isotopes. *Spectrochimica Acta Part B-Atomic Spectroscopy* **60**, 1402-1411 (2005).
12. Lama, F., Strain, J.A., Townsend, P.D., Bolus, D. & Mapper, D. ENERGY AND ANGULAR-DISTRIBUTION OF AR⁺ SPUTTERED UO₂. *Radiation Effects and Defects in Solids* **99**, 301-311 (1986).
13. Konomi, I., *et al.* Angular distribution of atoms emitted from a SrZrO₃ target by laser ablation under different laser fluences and oxygen pressures. *Journal of Vacuum Science & Technology A: Vacuum, Surfaces, and Films* **28**, 400-406 (2010).
14. Smalley, R.E., Wharton, L. & Levy, D.H. MOLECULAR OPTICAL SPECTROSCOPY WITH SUPERSONIC BEAMS AND JETS. *Accounts Chem. Res.* **10**, 139-145 (1977).

15. Mariella, R. ISOTOPE SHIFT IN THE 22P STATES OF LITHIUM AND SPATIALLY RESOLVED LASER-INDUCED FLUORESCENCE. *Applied Physics Letters* **35**, 580-582 (1979).
16. Isselhardt, B.H., *et al.* Improving Precision in Resonance Ionization Mass Spectrometry: Influence of Laser Bandwidth in Uranium Isotope Ratio Measurements. *Anal. Chem.* **83**, 2469-2475 (2011).
17. Citron, M.L., Gray, H.R., Gabel, C.W. & Stroud, C.R. POWER BROADENING OF ABSORPTION-SPECTRUM IN OPTICALLY ORIENTED SODIUM. *Journal of the Optical Society of America* **66**, 1068-1068 (1976).
18. Citron, M.L., Gray, H.R., Gabel, C.W. & Stroud, C.R. EXPERIMENTAL STUDY OF POWER BROADENING IN A 2-LEVEL ATOM. *Phys. Rev. A* **16**, 1507-1512 (1977).
19. Dikshit, B., Majumder, A., Bhatia, M.S. & Mago, V.K. Collisional effects on metastable atom population in vapour generated by electron beam heating. *Journal of Physics D-Applied Physics* **41**(2008).
20. Semerok, A.F., Vors, E., Wagner, J.F. & Fomichev, S.V. Non-selective photoionization of uranium atoms by the third harmonic of a Nd-YAG laser: experiment and simulation. *J. Phys. B-At. Mol. Opt. Phys.* **34**, 565-578 (2001).
21. Vors, E., Semerok, A., Wagner, J.F. & Fomichev, S.V. Non-selective photoionization for isotope ratio measurements by time of flight mass spectrometry with laser ablation. *Applied Surface Science* **168**, 166-169 (2000).
22. Donohue, D.L. & Young, J.P. Detection of Plutonium by Resonance Ionization Mass-Spectrometry. *Anal. Chem.* **55**, 378-379 (1983).
23. Donohue, D.L., Smith, D.H., Young, J.P., McKown, H.S. & Pritchard, C.A. Isotopic Analysis of Uranium and Plutonium Mixtures by Resonance Ionization Mass-Spectrometry. *Anal. Chem.* **56**, 379-381 (1984).
24. Capelle, G.A., Young, J.P., Donohue, D.L. & Smith, D.H. Laser Bandwidth Effects in Resonance Ionization Spectroscopy of Nd. *Journal of the Optical Society of America B-Optical Physics* **4**, 445-451 (1987).
25. Erdmann, N., *et al.* Determination of the first ionization potential of nine actinide elements by resonance ionization mass spectroscopy (RIMS). *Journal of Alloys and Compounds* **271**, 837-840 (1998).
26. Kohler, S., *et al.* Determination of the first ionization potential of actinide elements by resonance ionization mass spectroscopy. *Spectrochimica Acta Part B-Atomic Spectroscopy* **52**, 717-726 (1997).
27. Goeringer, D.E., Christie, W.H. & Valiga, R.E. Investigation of Matrix Effects On The Neutral Fractions Ejected From Ion-Bombarded, Uranium-Containing Solids Using Resonance Ionization Mass-Spectrometry. *Anal. Chem.* **60**, 345-349 (1988).
28. Knight, K.B., *et al.* Uranium resonance ionization mass spectrometry in natural U-silicate. *Proceedings in Radiochemistry* **1**, 37-43 (2011).
29. Gavrilescu, M., Pavel, L.V. & Cretescu, I. Characterization and remediation of soils contaminated with uranium. *Journal of Hazardous Materials* **163**, 475-510 (2009).
30. Khan, K. & Khan, H.M. Natural gamma-emiting radionuclides in Pakistani Portland cement. *Applied Radiation and Isotopes* **54**, 861-865 (2001).

31. Righi, S., Betti, M., Bruzzi, L. & Mazzotti, G. Monitoring of natural radioactivity in working places. *Microchem J.* **67**, 119-126 (2000).
32. Bruzzi, L., Mele, R. & Padoani, F. Evaluation of gamma and alpha doses due to natural radioactivity of building materials. *Journal of Radiological Protection* **12**, 67 (1992).
33. Pflieger, R., Colle, J.Y., Iosilevskiy, I. & Sheindlin, M. Urania vapor composition at very high temperatures. *Journal of Applied Physics* **109**, 33501-33501 (2011).
34. Chen, H.L. & Borzileri, C. COLLISIONAL RELAXATION OF LOW-LYING ELECTRONICALLY EXCITED-STATES OF URANIUM - F3DS2(5K05) AND (5L70)A). *Journal of Chemical Physics* **72**, 853-857 (1980).
35. Denecke, M.A., *et al.* Spatially resolved micro-X-ray fluorescence and micro-X-ray absorption fine structure study of a fractured granite bore core following a radiotracer experiment. *Spectrochimica Acta Part B-Atomic Spectroscopy* **64**, 791-795 (2009).
36. Denecke, M.A., *et al.* mu-X-ray fluorescence and mu-X-ray diffraction investigations of sediment from the Ruprechtov nuclear waste disposal natural analog site. *Spectrochimica Acta Part B-Atomic Spectroscopy* **63**, 484-492 (2008).
37. Popmintchev, T., *et al.* Bright Coherent Ultrahigh Harmonics in the keV X-ray Regime from Mid-Infrared Femtosecond Lasers. *Science* **336**, 1287-1291 (2012).
38. Lind, O.C., Salbu, B., Janssens, K., Proost, K. & Dahlgaard, H. Characterization of, uranium and plutonium containing particles originating from the nuclear weapons accident in Thule, Greenland, 1968. *Journal of Environmental Radioactivity* **81**, 21-32 (2005).
39. Erdmann, N., Kratz, J.V., Trautmann, N. & Passler, G. Resonance ionization mass spectrometry of ion beam sputtered neutrals for element- and isotope-selective analysis of plutonium in micro-particles. *Anal. Bioanal. Chem.* **395**, 1911-1918 (2009).
40. Ranebo, Y., *et al.* The use of SIMS and SEM for the characterization of individual particles with a matrix originating from a nuclear weapon. *Microscopy and Microanalysis* **13**, 179-190 (2007).
41. Eriksson, M., Lindahl, P., Roos, P., Dahlgaard, H. & Holm, E. U, Pu, and Am nuclear signatures of the Thule hydrogen bomb debris. *Environmental Science & Technology* **42**, 4717-4722 (2008).